nature nanotechnology

SUPPLEMENTARY INFORMATION

DOI: 10.1038/NNANO.2017.23

In the format provided by the authors and unedited.

DNA probes for monitoring dynamic and transient molecular encounters on live cell membranes

Mingxu You[†*], Yifan Lyu[†], Da Han[†], Liping Qiu, Qiaoling Liu, Tao Chen, Cuichen Sam Wu, Lu Peng, Liqin Zhang, Gang Bao and Weihong Tan[*]

[†]These authors contributed equally to this work.

*e-mail: tan@chem.ufl.edu; mingxuyou@chem.umass.edu

© 2017 Macmillan Publishers Limited, part of Springer Nature. All rights reserved.

1. Supplementary Methods.

Chemicals and reagents. The materials for DNA synthesis were purchased from Biosearch Technologies (Petaluma, CA) or Glen Research (Sterling, VA), including Quasar 670 phosphoramidite, cholesterol-TEG phosphoramidite, tocopherol-TEG phosphoramidite, 5'-stearyl phosphoramidite, 6-fluorescein phosphoramidite and TMR-dT phosphoramidite. The synthesis and characterization of diacyllipid phosphoramidite were performed in our group and have been reported previously[1]. Lipid molecules such as soybean polar extract, N-stearoyl-D-sphingomyelin (SSM), 1,2-dioleoyl-*sn*-glycero-3-phospho-1'-*rac*-glycerol (DOPG) and cholesterol were purchased from Avanti Polar Lipids, and stored in chloroform at -20 °C. Teflon AF solution (1601SOL, 6%) was purchased from Chemours. Other chemicals were purchased from Sigma-Aldrich. All reagents for buffer preparation and HPLC purification came from Fisher Scientific. Unless otherwise stated, all chemicals were used without further purification.

Cell lines. CCRF-CEM (CCL-119, T-cell line, human ALL) and Ramos (CRL-1596, B-cell line, human Burkitt's lymphoma) were cultured in RPMI 1640 medium (American Type Culture Collection) with 10% fetal bovine serum (Invitrogen, Carlsbad, CA) and 0.5 mg/mL penicillin-streptomycin (American Type Culture Collection) at 37°C under a 5% CO_2 atmosphere. Both cell lines were tested regularly for mycoplasma contamination. Cells were washed before and after incubation with washing buffer [4.5g/L glucose and 5 mM $MgCl_2$ in Dulbecco's PBS with calcium chloride and magnesium chloride (Sigma-Aldrich)]. Binding buffer was prepared by adding yeast tRNA (0.1mg/mL; Sigma-Aldrich) and BSA (1mg/mL; Fisher Scientific) to the washing buffer to reduce background binding.

© 2017 Macmillan Publishers Limited, part of Springer Nature. All rights reserved.

DNA synthesis. All oligonucleotides were synthesized using an ABI 3400 DNA synthesizer (Applied Biosystems, Inc., Foster City, CA) at the 1.0 μmol scale. After complete cleavage and deprotection, the DNA sequences were purified on a ProStar HPLC system (Varian, Palo Alto, CA) with a C-18 reversed-phase column (Alltech, 5μm, 250mm × 4.6 mm). Diacyllipid-ODN was synthesized by extended coupling time (900 seconds). After synthesis, the DNA was cleaved and deprotected from the CPG and purified by reversed phase HPLC using a C4 column (BioBasic-4, 200mm x 4.6mm, Thermo Scientific). The eluent was 100mM triethylamine-acetic acid buffer (TEAA, pH 7.5) and acetonitrile (0-30min, 10-100%). All DNA concentrations were characterized with a Cary Bio-300UV spectrometer (Varian) using the absorbance of DNA at 260nm.

Characterization of DNA probe functions. A FluoroMax-4 Spectrofluorometer with a temperature controller (Jobin Yvon) was used for the steady-state and kinetic fluorescence measurements. The preannealed DNA duplexes **S1/B** and **S2/W** were prepared by a cooling process from 95 °C to 25 °C over a period of 30 min in a 1× PBS buffer (12 mM, pH=7.4 with 137 mM NaCl and 2.7 mM KCl). The strand displacement reactions were analyzed by mixing 50nM oligonucleotides or duplexes in 1× PBS buffer, and the fluorescence emission at 515 nm (6-carboxyfluorescein) was recorded using an excitation wavelength of 488 nm (slit width set as 3 nm, 0.1 s interval time).

Measurement of internalization efficiency of the DNA probe. A 6-carboxyfluorescein-labeled reporter probe was added to calculate the amount of its complementary strand on the cell surface after a series of cellular incubation times[2]. Since the negatively charged phosphate groups of oligonucleotides prevented the reporter probes from being taken up by cells at 4 °C, the cell surface-anchored strands, but not the internalized strands, were hybridized and labeled in this way. Internalization efficiencies of 150 nM cholesterol-ODN, 300 nM diacyllipid-ODN, 400 nM

© 2017 Macmillan Publishers Limited, part of Springer Nature. All rights reserved.

tocopherol-ODN, 100 nM TC01-ODN, 400 nM TD05-ODN, 600 nM TE02-ODN and 0.1μM Sgc4f-ODN were tested with 5×10^5 Ramos cells/mL; the corresponding fluorescence changes were monitored by flow cytometry by adding two-fold 6-carboxyfluorescein-labeled **W** probe after a series of incubation times.

© 2017 Macmillan Publishers Limited, part of Springer Nature. All rights reserved.

2. Supplementary Table.

Supplementary Table 1: DNA sequences employed in this study. The nucleotides in color represent toehold regions to initiate strand displacement reactions; toeholds of the same color-can hybridize to each other.

Name	Sequence
I	5'- CTACGTCTACCCTACCACTACA -3'
C	5'- TGTAGTGGTAGGGTAGACGTAG-**Biotin** -3'
S1-Dcl	5'- TTTTT TTTTT-**Dabcyl**-TCACTCATTCAATACCCTACGTCTACCCTAC -3'
S2	5'- TTTTT TTTTT TCACTCATTCAATACC -3'
W-TMR	5'- GACGTAGGGTATTGAATGAGTGA-**TAMRA** -3'
W-FAM	5'- GACGTAGGGTATTGAATGAGTGA-**FAM** -3'
W-670	5'- GACGTAGGGTATTGAATGAGTGA-**Quasar 670** -3'
W2-FAM	5'- TGAGTGAATATTTGTGATGTCCA-**FAM** -3'
C-S1	5'- Cholesterol-TTTTT TTTTT TCACTCATTCAATACCCTACGTCTACCCTAC -3'
C-S1-Dcl	5'- Cholesterol-TTTTT TTTTT-**Dabcyl**-TCACTCATTCAATACCCTACGTCTACCCTAC -3'
C-S1-BHQ2	5'- Cholesterol-TTTTT TTTTT-**BHQ-2**-TCACTCATTCAATACCCTACGTCTACCCTAC -3'
C-S2	5'- Cholesterol-TTTTT TTTTT TCACTCATTCAATACC-3'
L-S1	5'- Lipid-TTTTT TTTTT TCACTCATTCAATACCCTACGTCTACCCTAC -3'
L-S1-Dcl	5'- Lipid-TTTTT TTTTT-**Dabcyl**-TCACTCATTCAATACCCTACGTCTACCCTAC -3'
L-S2	5'- Lipid-TTTTT TTTTT TCACTCATTCAATACC -3'
T-S1	5'- Tocopherol-TTTTT TTTTT TCACTCATTCAATACCCTACGTCTACCCTAC -3'
T-S1-Dcl	5'- Tocopherol-TTTTT TTTTT-**Dabcyl**-TCACTCATTCAATACCCTACGTCTACCCTAC -3'
T-S2	5'- Tocopherol-TTTTT TTTTT TCACTCATTCAATACC -3'
C_1	5'- Cholesterol-TTTTT TTTTT TCACTCATTCAATACCCTACGTCTACCCTAC -3'
C_2-Dcl	5'- Cholesterol-TTTTT TTTTT-**Dabcyl**-TGGACATCACAAATATTCACTCATTCAATACC -3'
C_3	5'- Cholesterol-TTTTT TTTTTTGGACATCACAAATAT -3'
Sgc4f-S1-Dcl	5'- ATCACTTATAACGAGTGCGGATGCAAACGCCAGACAGGGGGACAGGAGATAAGTGA TTTTT TTTTT-**Dabcyl**-TCACTCATTCAATACCCTACGTCTACCCTAC -3'
Sgc4f-S2	5'- ATCACTTATAACGAGTGCGGATGCAAACGCCAGACAGGGGGACAGGAGATAAGTGA TTTTT TTTTT TCACTCATTCAATACC -3'
Sgc8-S1-Dcl	5'-ATCTAACTGCTGCGCCGCCGGGAAAATACTGTACGGTTAGA TTTTT TTTTT-**Dabcyl**-TCACTCATTCAATACCCTACGTCTACCCTAC -3'
TE02-S1-Dcl	5'-TAGGCAGTGGTTTGACGTCCGCATGTTGGGAATAGCCACGCCT TTTTT TTTTT-**Dabcyl**-TCACTCATTCAATACCCTACGTCTACCCTAC -3'
TE02-S2	5'-TAGGCAGTGGTTTGACGTCCGCATGTTGGGAATAGCCACGCCT TTTTT TTTTT TCACTCATTCAATACC -3'
TD05-S1-Dcl	5'-AGGAGGATAGTTCGGTGGCTGTTCAGGGTCTCCTCCT TTTTT TTTTT-**Dabcyl**-TCACTCATTCAATACCCTACGTCTACCCTAC -3'
TD05-S2	5'-AGGAGGATAGTTCGGTGGCTGTTCAGGGTCTCCTCCT TTTTT TTTTT TCACTCATTCAATACC -3'
TC01-S1-Dcl	5'-ACCAAACACAGATGCAACCTGACTTCTAACGTCATTTGGT TTTTT TTTTT-**Dabcyl**-TCACTCATTCAATACCCTACGTCTACCCTAC -3'
TC01-S2	5'-ACCAAACACAGATGCAACCTGACTTCTAACGTCATTTGGT TTTTT TTTTT TCACTCATTCAATACC -3'

© 2017 Macmillan Publishers Limited, part of Springer Nature. All rights reserved.

3. Supplementary Figures.

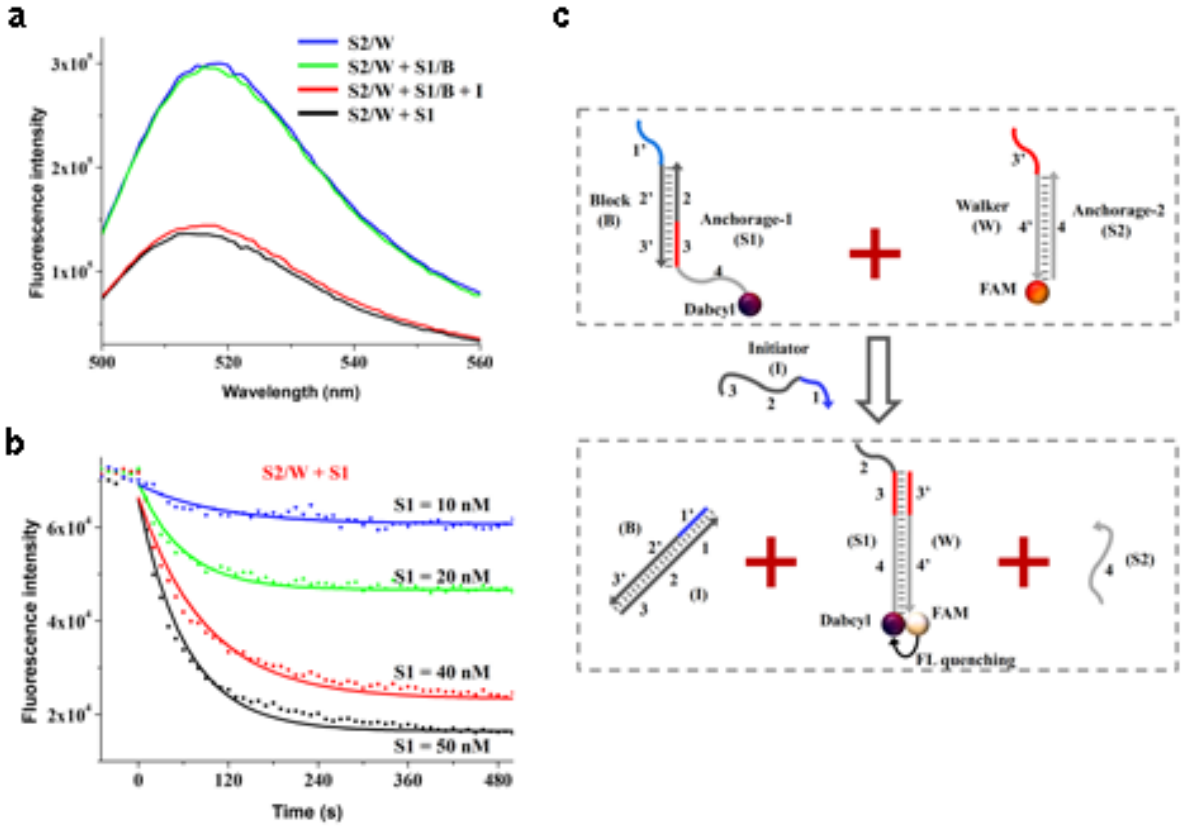

Supplementary Fig. 1: Characterization and performance of DNA probes. Strand displacement efficiency in 1× PBS buffer was studied by (a) fluorescence of 50 nM of each strand after 10 min reaction and (b) kinetic measurements after mixing **S1** strands of various initial concentrations with 50 nM **S2**/**W** probes. (c) The scheme illustrates the fluorescence signaling process for these studied strand displacement reactions.

© 2017 Macmillan Publishers Limited, part of Springer Nature. All rights reserved.

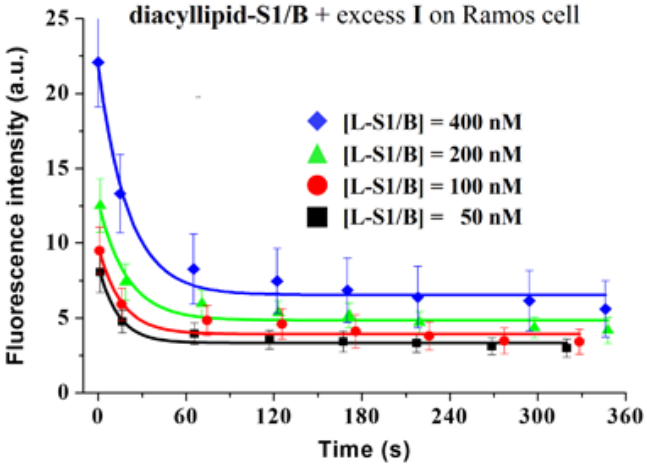

Supplementary Fig. 2: The kinetics of block removal on the Ramos cell membrane. Twenty-fold **I** strand was added each time, followed by measuring the mean fluorescence of 5,000 cells for each spot.

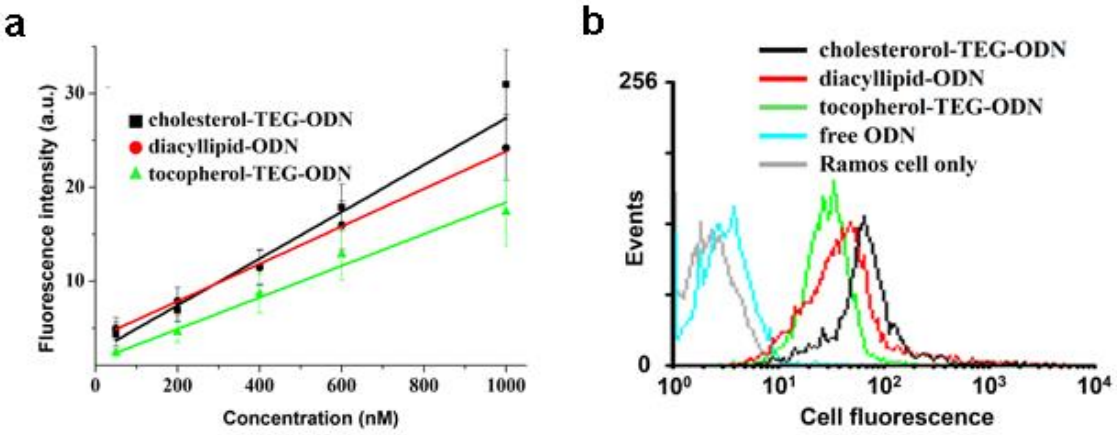

Supplementary Fig. 3: Flow cytometry evaluation of modification efficiency of different anchor-oligonucleotide conjugates on individual cell membranes. (a) Membrane anchoring efficiency on the CCRF-CEM cell surface; (b) Modification efficiencies on the Ramos cell surface.

© 2017 Macmillan Publishers Limited, part of Springer Nature. All rights reserved.

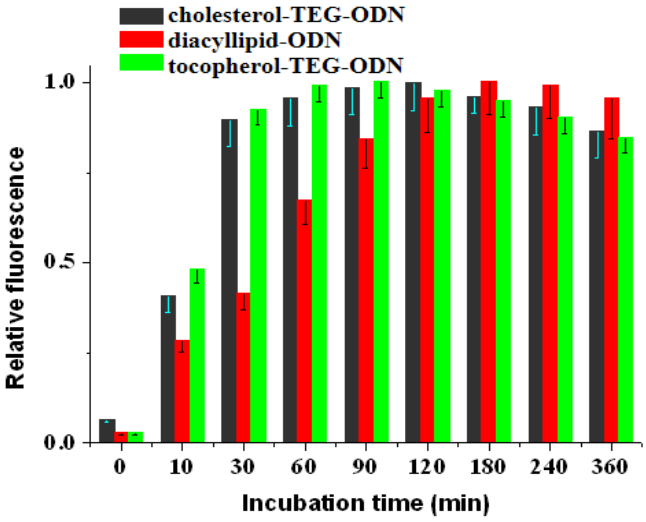

Supplementary Fig. 4: Internalization efficiencies of 150 nM cholesterol-ODN, 300 nM diacyllipid-ODN and 400 nM tocopherol-ODN by 5×10^5 Ramos cells/mL. Two-fold 6-carboxyfluorescein-labeled **W** probe was added after a series of incubation times. Since the negatively charged phosphate groups of oligonucleotides prevented the reporter probes from being taken up by cells, only the cell surface-anchored strands, but not the internalized strands, were hybridized and labeled in this way. Relatively low fluorescence level during the first 10 min of incubation is due to the slow cell membrane insertion kinetics of the oligonucleotide probes. During this 10 min, oligonucleotide probes still didn't reach membrane insertion equilibrium, and were still mainly in solution.

© 2017 Macmillan Publishers Limited, part of Springer Nature. All rights reserved.

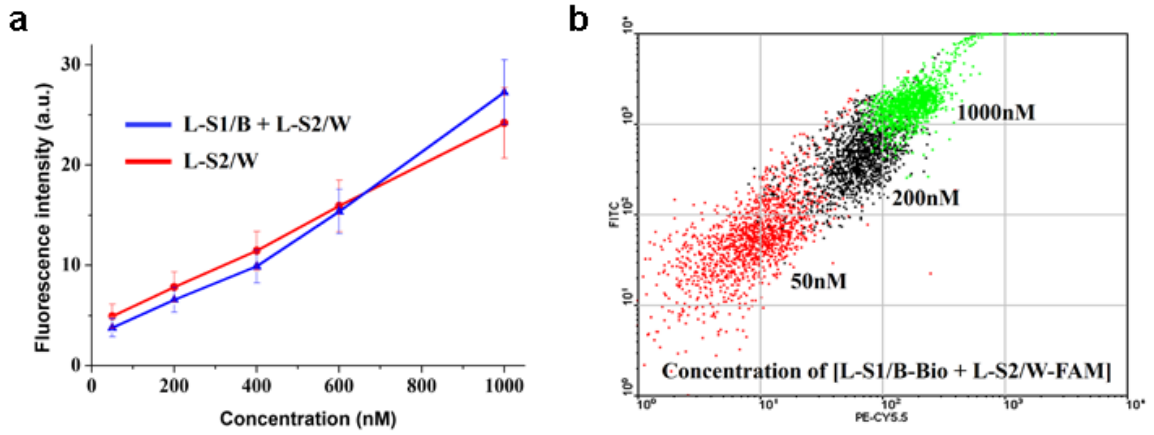

Supplementary Fig. 5: (a) Colocalization of diacyllipid-modified **S1/B** and **S2/W**-FAM conjugates on the Ramos cell membrane. (b) Dot graph showing individual cell modification, where the X-axis represents the relative anchoring efficiency of biotin-linked diacyllipid-**S1/B** conjugates with streptavidin-conjugated PE-Cy5.5 labeling, and the Y-axis represents the anchoring of FAM-labeled diacyllipid-**S2/W** conjugates.

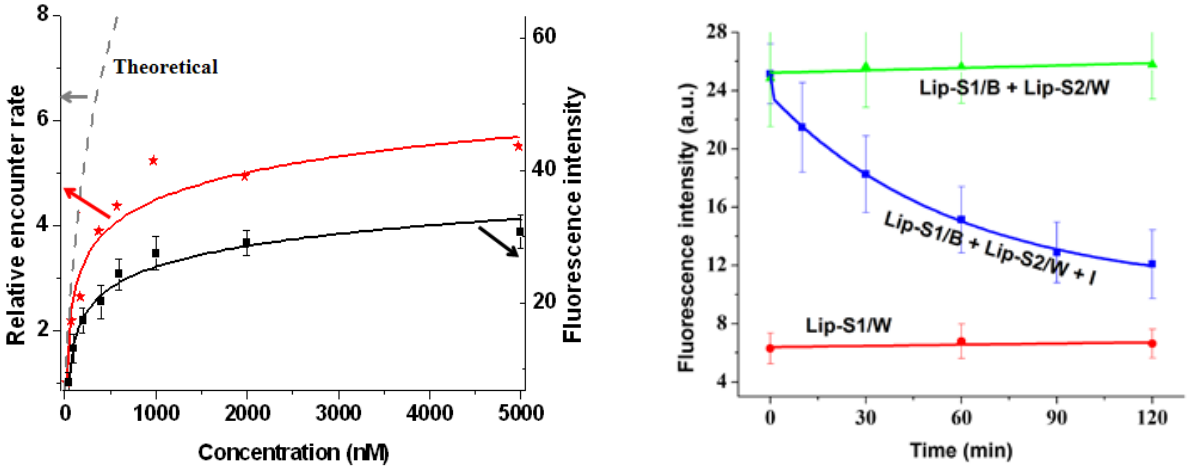

(Continued on the next page)

© 2017 Macmillan Publishers Limited, part of Springer Nature. All rights reserved.

Name	Sequence
$C_{0,5,10}$-S1	5'- Cholesterol-**(T)$_{0,5,10}$ -Dabcyl**-TCACTCATTCAATACCCTACGTCTACCCTAC -3'
$C_{0,5,10}$-S2	5'- Cholesterol-**(T)$_{0,5,10}$** TCACTCATTCAATACC-3'
$L_{0,5,10}$-S1	5'- Diacyllipid-**(T)$_{0,5,10}$ -Dabcyl**-TCACTCATTCAATACCCTACGTCTACCCTAC -3'
$L_{0,5,10}$-S2	5'- Diacyllipid-**(T)$_{0,5,10}$** TCACTCATTCAATACC -3'

Lipid pair	Relative encounter rate	Lipid pair	Relative encounter rate
C_0-S1/ L_0-S2	Too slow to be calculated	L_0-S1/ C_0-S2	0.28 ± 0.06
C_5-S1/ L_5-S2	0.62 ± 0.10	L_5-S1/ C_5-S2	1.22 ± 0.17
C_{10}-S1/ L_{10}-S2	1.02 ± 0.16	L_{10}-S1/ C_{10}-S2	1.51 ± 0.15

Supplementary Fig. 6: (upper left) Relative encounter rates between two diacyllipid-conjugated anchorages at different initial probe concentrations. The dashed theoretical curve represents the condition for which the apparent locomotion rate constant k″ is independent of DNA probe membrane density. (Upper right) Locomotion of DNA probe between two diacyllipid-conjugated anchorage sites with 5×10^5 CCRF-CEM cells/mL; 300 nM of each probe were added initially. The solid lines in the figures are the fitted curves based on the bimolecular interaction model. (Bottom) The effect of DNA spatial availability on strand displacement efficiency. Three linkers of different flexibilities and lengths, including 0, 5, and 10 nucleotide-long thymine linkers, were prepared. The sequence of each studied DNA probe is shown in the table. The use of a longer, more flexible 10-thymine linker resulted in improved DNA strand spatial availability, more symmetry results in the relative encounter rates around the diagonal lipids, and reduced spatial constraint from anchoring of different lipids. To further control for this DNA orientation-induced strand displacement efficiency variation, strategies using even more flexible linkers (e.g., long PEG linker) might be useful. One advantage of these DNA-based probes is the straightforward nature of chemical synthesis, along with diverse choice of modification.

© 2017 Macmillan Publishers Limited, part of Springer Nature. All rights reserved.

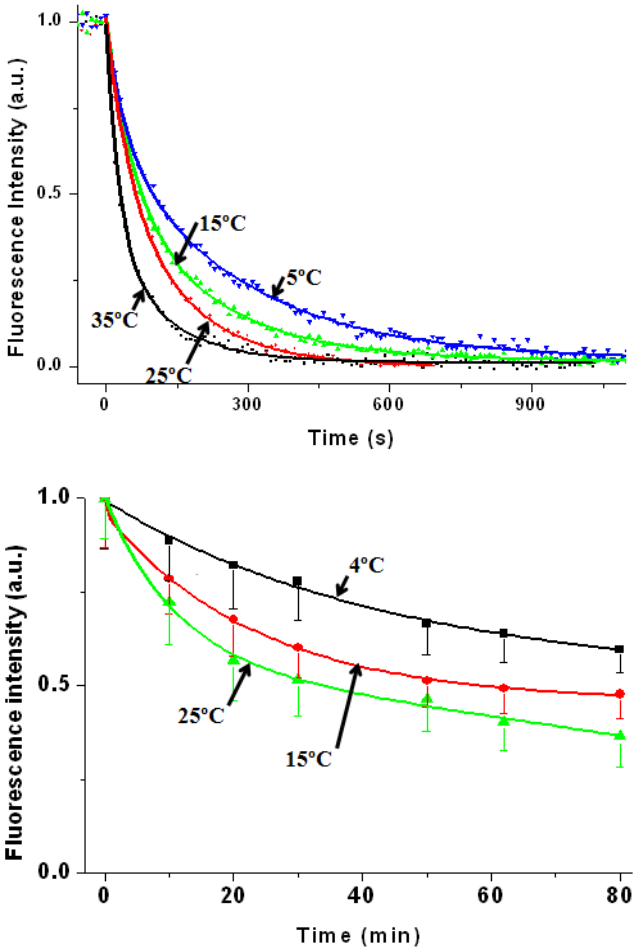

Supplementary Fig. 7: The effect of temperature on strand displacement efficiency. (Top) The kinetic measurements were studied in 1× PBS buffer by mixing 50 nM Dabcyl-modified S1 strands with 50 nM **S2**/**W**-FAM probes at different temperatures. (Bottom) The encounter event between diacyllipid-**S1** and diacyllipid-**S2** was studied on the surface of Ramos cells (5×10^5 /mL). The immobilization of 300 nM each diacyllipid-ODN was first realized at room temperature; then three flow tubes were separately incubated at different temperatures and monitored by measuring the mean fluorescence of 5,000 cells at a series of times using flow cytometry. Since the DNA strand migration step (step 3 in Fig. 1a, 10-100 μs/base) is much faster compared with the diffusion step (step 2 in Fig. 1a), such temperature effect was believed to be mainly a result of the change in the diffusion step, rather than the strand displacement reaction itself.

© 2017 Macmillan Publishers Limited, part of Springer Nature. All rights reserved.

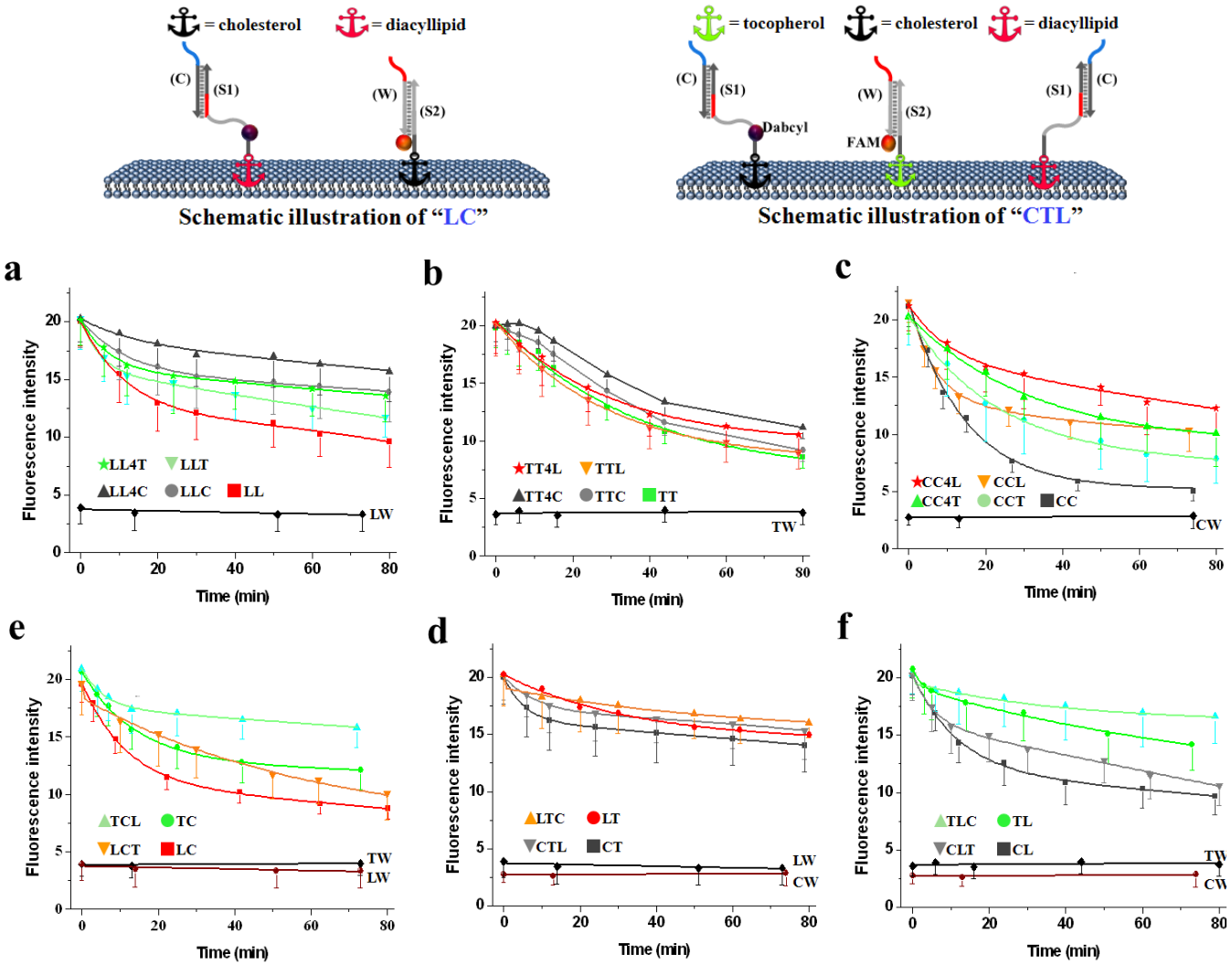

Supplementary Fig. 8: Competition experiments for studying the preference of ligand-ligand encounter. The encounter studies involved 150 nM cholesterol-ODN, 300 nM diacyllipid-ODN and 400 nM tocopherol-ODN with 5×10^5 Ramos cells/mL. Each sample was separated into two tubes, with or without the addition of a 20-fold excess of **I** strand. Both tubes were monitored by measuring the mean fluorescence of 5,000 cells after a series of times using flow cytometry. The displayed plot is the result after correcting for the fluorescence decay from the control tube without **I** strand.

© 2017 Macmillan Publishers Limited, part of Springer Nature. All rights reserved.

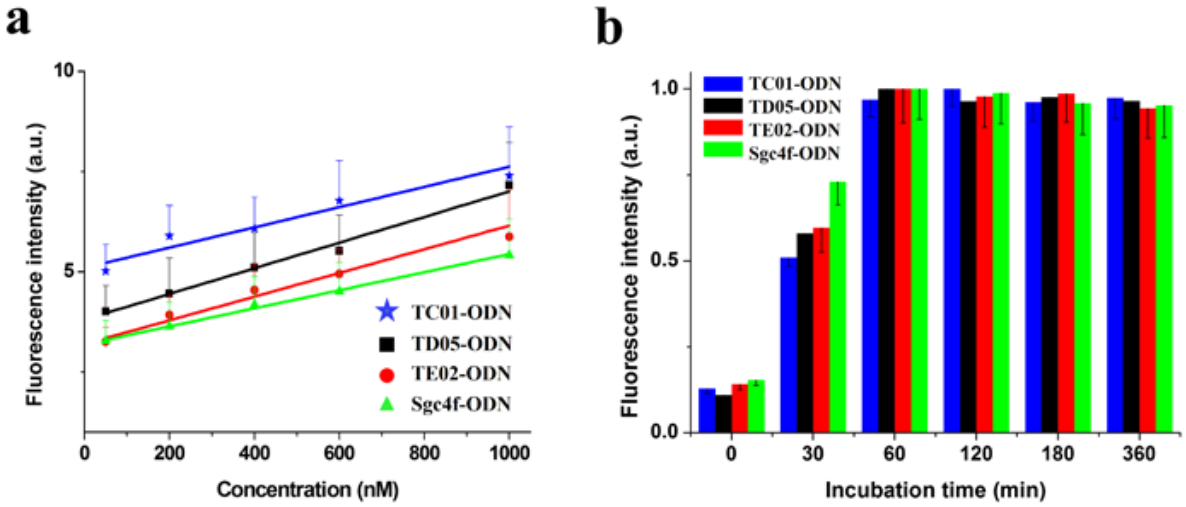

Supplementary Fig. 9: (a) Flow cytometry evaluation of modification efficiency of different aptamer anchor- oligonucleotide conjugates on the membrane of 5×10^5 Ramos cells/mL. (b) Internalization efficiencies of 100 nM TC01-ODN, 400 nM TD05-ODN, 600 nM TE02-ODN or 1000 nM Sgc4f-ODN with two-fold 6-carboxyfluorescein-labeled **W** probe added after a series of incubation times.

© 2017 Macmillan Publishers Limited, part of Springer Nature. All rights reserved.

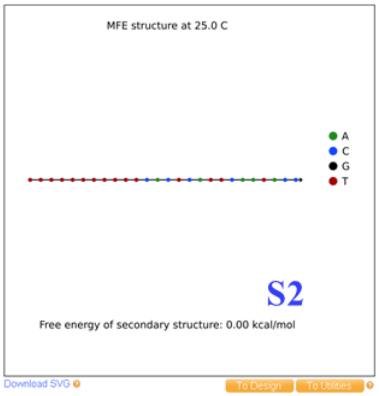

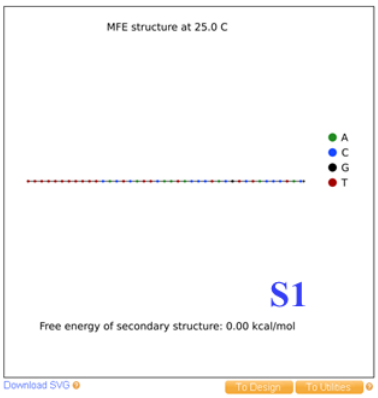

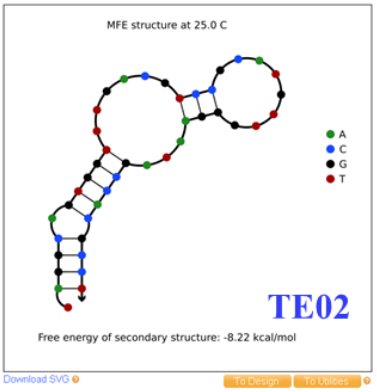

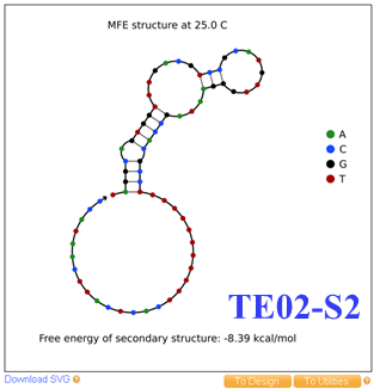

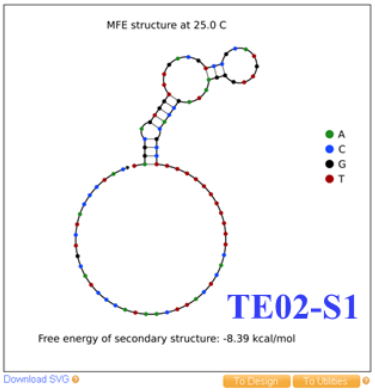

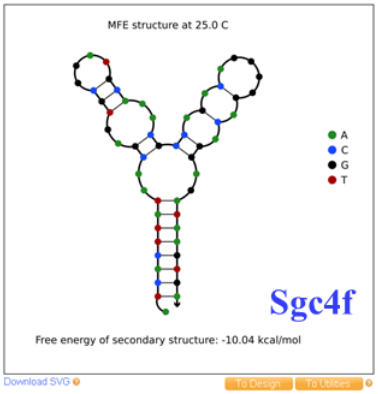

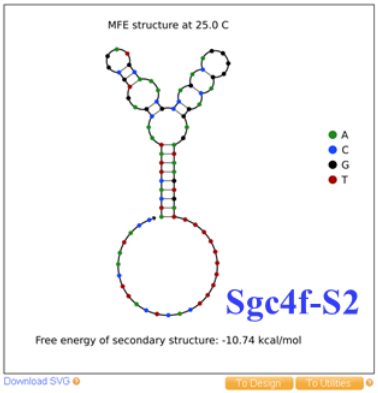

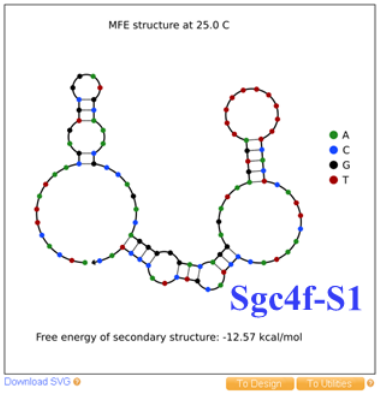

(Continued on the next page)

© 2017 Macmillan Publishers Limited, part of Springer Nature. All rights reserved.

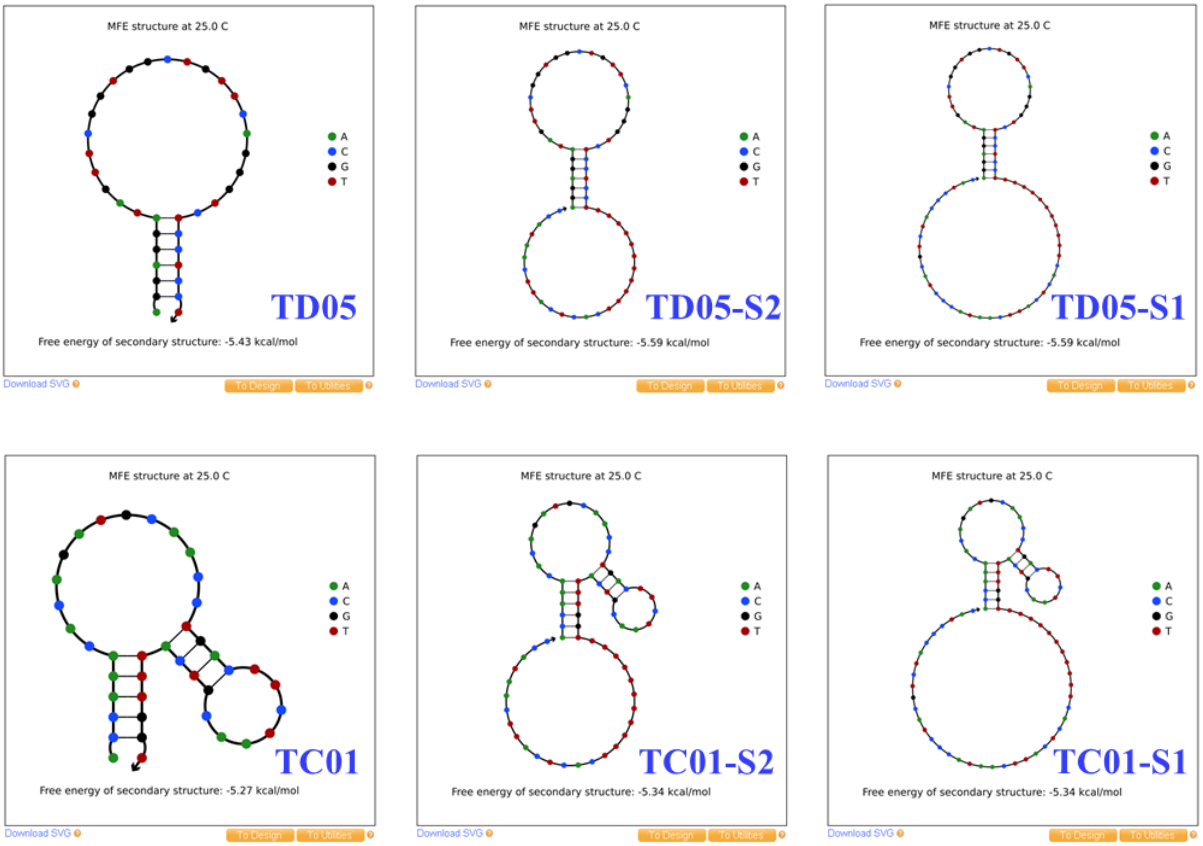

Supplementary Fig. 10: Thermodynamic prediction of the secondary structures of aptamer-oligonucleotide conjugates, using NUPACK and IDT Oligo Analyzer software. The predicted secondary structure of each modified aptamer is shown here. Compared with their original structures or free energies, no obvious change was observed, with the exception of Sgc4f-**S1** conjugate which showed some variation. However, considering the small free energy change, such variation would not significantly affect the binding affinity of Sgc4f aptamer.

© 2017 Macmillan Publishers Limited, part of Springer Nature. All rights reserved.

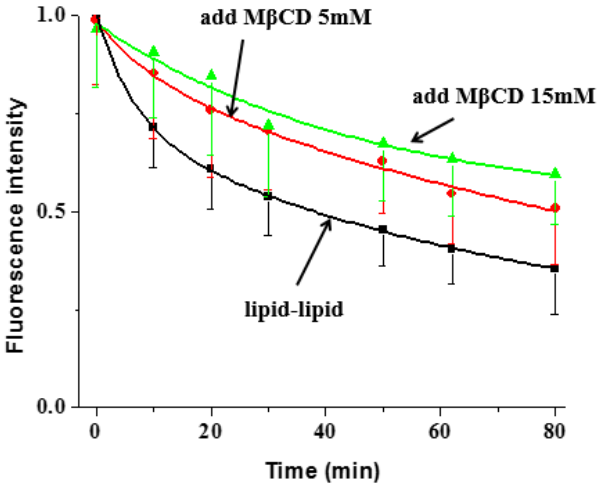

Supplementary Fig. 11: The effect of cholesterol density on membrane interactions between diacyllipids. Cholesterol composition plays an important role in the formation of lipid domains. The lipid domain theory holds that the encounters of membrane molecules critically depend on their interactions with neighboring molecules, thus explaining the concept of preferential encounters[3]. By adding methyl-β-cyclodextrin to selectively extract cholesterols from the Ramos cell membrane[4], we studied the effect of cholesterol densities on the membrane encounter rates between diacyllipids. In our experiment, 5 mM or 15 mM methyl-β-cyclodextrin (MβCD) was used to selectively extract cholesterols for 15 minutes from Ramos cell surfaces at 37 °C. A clearly slower diacyllipid-diacyllipid encounter after cholesterol extraction was observed. This experiment indicates that lipid encounter rate is indeed influenced by neighbor cholesterol molecules in the lipid domain. To study the effect of cholesterol extraction in the membrane diffusion rate of diacyllipid, we performed fluorescence recovery after photobleaching measurements before and after the removal of cholesterol. Indeed, the addition of 15 mM methyl-β-cyclodextrin reduced the diffusion coefficient of diacyllipid, from 0.86 ± 0.12 $\mu m^2/s$ to 0.45 ± 0.09 $\mu m^2/s$. This result indicates that the observed reduction in diacyllipid encounter rates could be mainly due to the reduced diffusion rate change after the removal of cholesterol.

© 2017 Macmillan Publishers Limited, part of Springer Nature. All rights reserved.

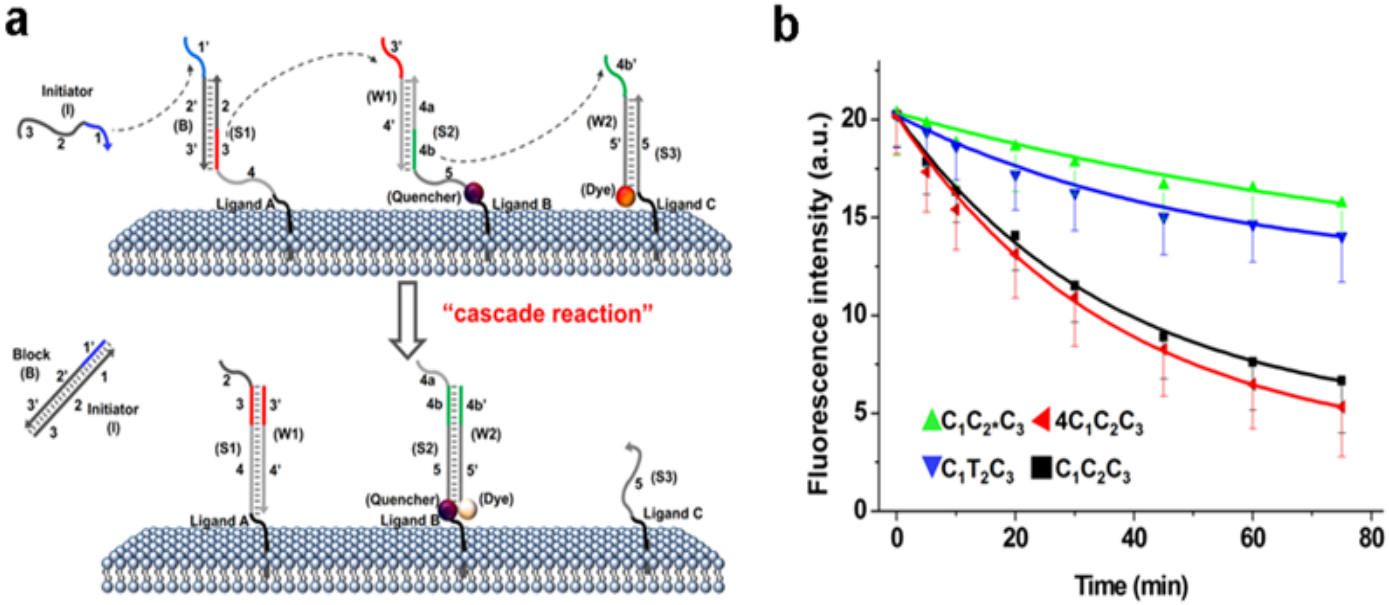

Supplementary Fig. 12: DNA probe to study multicomponent encounters in a cascade pathway. (a) Simplified scheme of programmable membrane cascade encounters. The dash lines indicate the toehold recognition positions that can initiate strand displacements. (b) Locomotion of DNA probe W2 in the cascade pathways as monitored with flow cytometry. Initially, 150 nM of each cholesterol (**C**)-anchored conjugate, or 400 nM of each tocopherol (**T**)-anchored conjugate were incubated with 5×10^5 Ramos cells/mL. It should be noted that 4-fold $\mathbf{C_1}$ probes (600 nM) were added for "$\mathbf{4C_1C_2C_3}$" in an attempt to speed up the reactions. $\mathbf{C_{2^*}}$ probe was employed as a control to inhibit the locomotion of probe **W2** by a noncomplementary **S2*** strand. In another case, we changed the cholesterol-conjugated $\mathbf{C_2}$ site into a disfavored encounter component: tocopherol-conjugated $\mathbf{T_2}$ site. In this case, locomotion of the **W2** strand from **S3** to **S2** site was significantly slowed down. All experiments were repeated at least three times. The error bar stands for the standard deviation from 5,000 cell events at each time point.

Many signaling networks involve more than two membrane components, mostly in a cascade pathway. For instance, in a signal transduction cascade, a ligand recognition event induces a series

© 2017 Macmillan Publishers Limited, part of Springer Nature. All rights reserved.

of successive encounter and reaction rate variations among receptors and other membrane components. Based on this result, the programmability of DNA strand displacement reactions has allowed us to study DNA probe locomotion relative to multicomponent encounters in a cascade pathway. For example, the motion of DNA probe **W1** from cholesterol-anchored $\mathbf{C_2}$ to site $\mathbf{C_1}$ can be controlled to initiate a cascade operation which, in turn, results in the locomotion of the secondary walker **W2** from $\mathbf{C_3}$ to $\mathbf{C_2}$ site (Fig. S12a). It should be recalled that we had previously fine-tuned the DNA probe by introducing a block strand (**B**) and an initiator strand (**I**). The block strand prevents strand displacement, and the initiator strand removes the block strand by a strand displacement reaction (Fig. 1a). In this way, DNA probe locomotion can be triggered only after the addition of **I**, thus allowing precise regulation over locomotion. Accordingly, in the operation described above, **W1** functions as a block strand to block the **W2**-recognizing toehold region in the $\mathbf{C_2}$ site. Only after the motion of **W1**, can the **W2**/$\mathbf{C_2}$ conjugate form through a strand displacement reaction. Using dye-labeled **W2** strand, the overall cascade encounter rate can be measured with flow cytometry (Fig. S12b). To study the impact of a different intermediate component on the overall cascade encounter rate, we changed the cholesterol-conjugated $\mathbf{C_2}$ site into a disfavored encounter component: tocopherol-conjugated $\mathbf{T_2}$ site. In this case, locomotion of the **W2** strand was significantly hindered (Fig. S12b). These findings indicate that the DNA probe can be used to study more complex membrane cascade encounter pathways.

© 2017 Macmillan Publishers Limited, part of Springer Nature. All rights reserved.

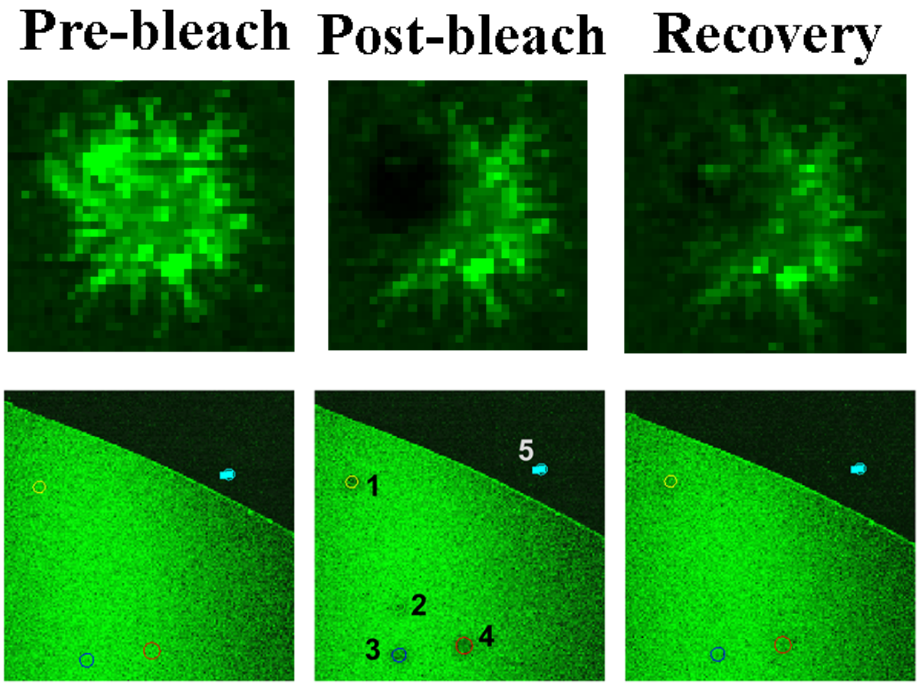

Type of lipid and membrane	D ± S.E. (μm²/s)
Diacyllipid-DNA on Ramos cell membrane	0.86 ± 0.12
Cholesterol-DNA on Ramos cell membrane	1.2 ± 0.2
Tocopherol-DNA on Ramos cell membrane	1.7 ± 0.3
Stearyl-DNA on model lipid monolayer	0.62 ± 0.03

Supplementary Fig. 13: Fluorescence recovery after photobleaching (FRAP) was used to study lateral diffusion of FITC-DNA-modified lipids on the (top) Ramos cell membrane and (bottom) model lipid monolayer film. A Zeiss LSM 880 laser scanning confocal microscope was used for the measurement. Membrane region of interest (a circular patch with diameter of 5-10 μm) was rapidly photo-bleached using high laser intensity (50%) at 488 nm. FRAP in the numbered region 1-4 of the model lipid monolayer film was averaged to calculate the diffusion coefficient, with region 5 as a control in the non-lipid region. The diffusion coefficient for each lipid was determined on the basis of a previous report[5].

© 2017 Macmillan Publishers Limited, part of Springer Nature. All rights reserved.

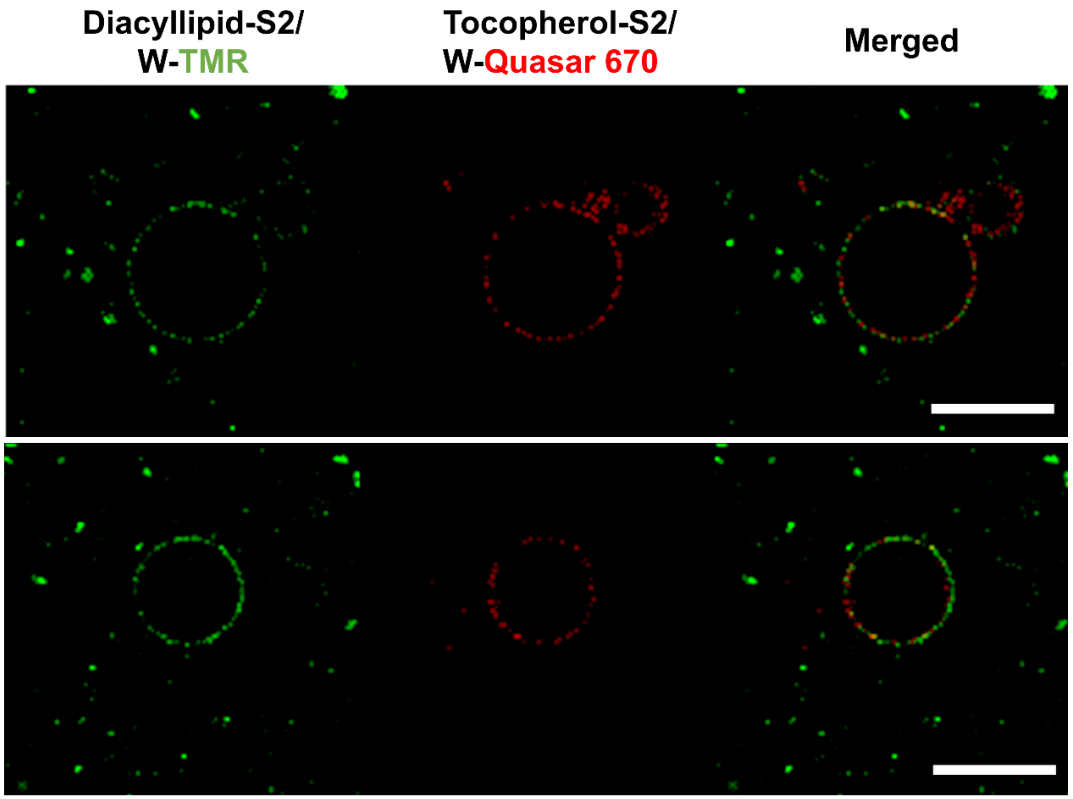

Supplementary Fig. 14: Lateral distribution of the diacyllipid- and tocopherol-anchored DNA duplexes in the domain-forming giant unilamellar vesicles (GUV). These GUVs, made of 1:1:1 DOPG/SSM/Chol at 100 μM lipid concentration, were synthesized following a modified protocol based on reference 14. Diacyllipid- and tocopherol-anchored DNA duplexes were added at a lipid to DNA molar ratio of 1000 to 1. The panels show representative fluorescence microscopy images of TMR-labeled diacyllipid-DNA duplex (green), Quasar 670-labeled tocopherol-DNA duplex (red) and an overlap of the images. Scale bar represents 10 μm. Colocalization analysis of the green and red pixel was performed using Coloc2 plugin in the Fiji software. Person's correlation coefficients (0.22 ± 0.04, mean ± S.E.) indicate the well separation of diacyllipid-DNA from tocopherol-DNA on the GUV membrane. Tocopherol-DNA is known to be mainly localized in the liquid-disordered ($\mathbf{l_d}$) domain[14], this experiment supports the preference of diacyllipid-DNA partition in the liquid-ordered ($\mathbf{l_o}$) domain.

© 2017 Macmillan Publishers Limited, part of Springer Nature. All rights reserved.

Supplementary Discussion 1: Temporal resolution of the DNA probe system.

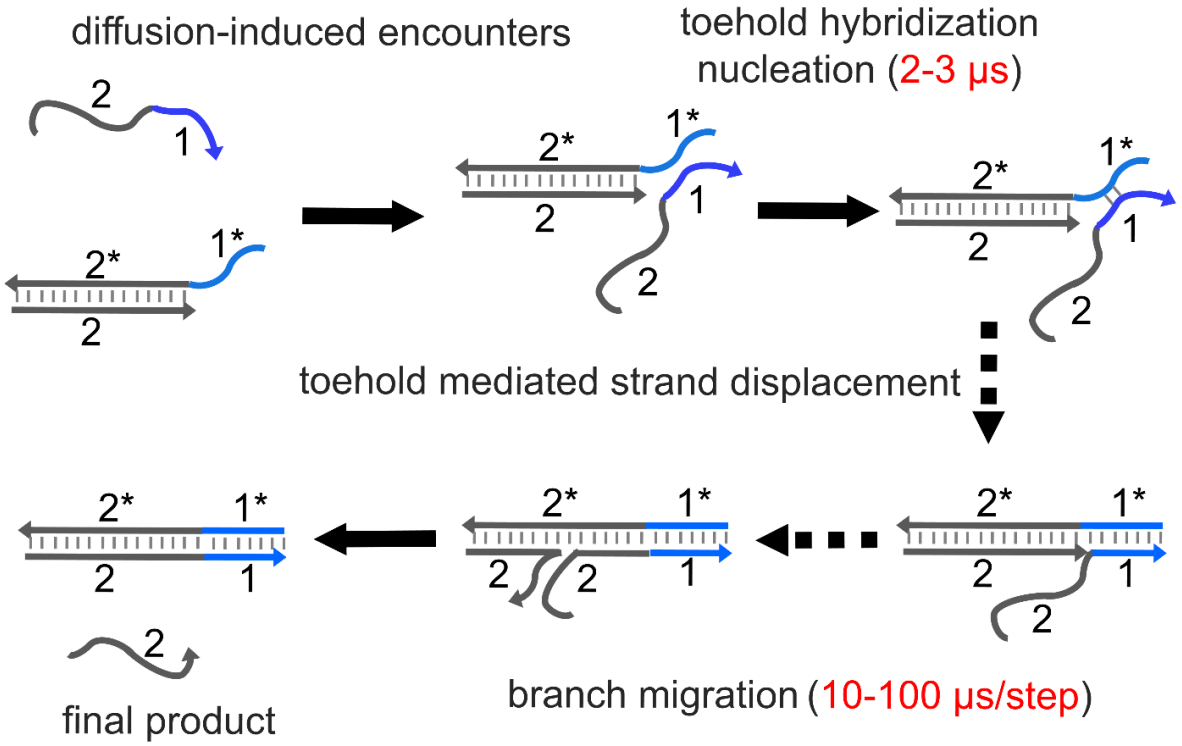

The temporal resolution of our method is estimated in the microsecond range. Encounters among membrane lipids are believed to occur in the same time scale[6]. As shown in the above scheme, the resolution of our method is limited by the kinetics of DNA hybridization nucleation (2-3 μs), i.e., the formation of the first few base pairs in the toehold region[7]. After the successful formation of the first few base pairs, strand migration reactions happen at the speed of 10-100 μs/step[8]. While this represents a relatively slow kinetics, this step does not determine the temporal resolution of our method. This is true as long as the encounter between two membrane molecules is long enough (several μs) to initiate hybridization nucleation. Under these conditions, hybridization of the first few base pairs will further strengthen hybridization and thus facilitate the following strand migration reactions[7,8]. As a result, our method can be used to study rapid microsecond-range encounters.

© 2017 Macmillan Publishers Limited, part of Springer Nature. All rights reserved.

Supplementary Discussion 2: Calculation of membrane lipid encounter rates.

We first try to solve the strand displacement reaction probability, P, after an **S1** and **W/S2** encounter on two-dimensional membrane. A stearyl-DNA-incorporated lipid monolayer film was prepared for this purpose[13]. Since stearyl-DNA can freely diffuse along the whole lipid membrane, the encounter rate will follow a two-dimensional Smoluchowski equation[11], where $F = 2\pi N_a C^2(D_1 + D_2)/\ln[(\pi N_a C)^{-1/2}/a]$. Here, "a" is the encounter radius two DNA probes must reach in order to react, and such radius is estimated to be around 5 nm for toehold-mediated strand displacement reactions[9,10]. "D_1" and "D_2" are the respective diffusion coefficients of each lipid molecule on the membrane, which was measured to be 0.62 ± 0.03 $\mu m^2/s$ based on the FRAP experiment. "C" is the concentration of lipids on the cell membrane, which was estimated to be about 0.32 $pmol/cm^2$. Based on this model, the encounter rate of two stearyl-DNA on model lipid membrane, F, was calculated to be 12 ± 1 per μm^2 per second. The encounter rate can be also interpreted based on effective fluorescence signal change and strand displacement reaction probability, $F = k''C^2/P$ (equation 5, see Methods). Here, k'' is the calculated effective locomotion rate constant from fluorescence microscopy measurement, which equals to $(1.6 \pm 0.2) \times 10^3$ cm^2 $pmol^{-1}$ s^{-1}. As a result, the strand displacement reaction probability, P, after an **S1** and **W/S2** encounter on two-dimensional membrane was calculated to be 0.032 ± 0.003. Interestingly, a recent study of DNA hybridization on a model lipid membrane reports a similar P = 0.034 reaction probability after membrane encounter involving complementary DNA strands of 20-nt in length[13].

Next, we tried to calculate lipid encounter rates on Ramos cell membrane. Membrane fluorescence intensity was calculated following a previous report[2]. The Ramos cell diameter was measured to be 12 ± 1 μm. The averaged concentration of DNA-modified lipids, C, on each cell membrane was estimated to be about 0.19 $pmol/cm^2$. Based on equation 5 (see Methods), the

© 2017 Macmillan Publishers Limited, part of Springer Nature. All rights reserved.

membrane encounter rate, F, can be calculated as $F = k''C^2/P$. Thus, based on the measured effective locomotion rate constant, k'', we can calculate the membrane encounter rates of each studied lipid pair, as summarized in the following table.

	Encounter rate (per μm^2 per sec)	Number of encounters across cell membrane (per millisecond)
Diacyllipid / Diacyllipid	19 ± 4	35 ± 7
Diacyllipid / Cholesterol	25 ± 4	45 ± 7
Diacyllipid / Tocopherol	4.3 ± 0.6	8.5 ± 1.2
Cholesterol / Cholesterol	48 ± 6	89 ± 11
Cholesterol / Tocopherol	6.3 ± 1.0	12 ± 2
Tocopherol / Tocopherol	16 ± 4	30 ± 6

© 2017 Macmillan Publishers Limited, part of Springer Nature. All rights reserved.

Supplementary Discussion 3: Cell membrane effective concentration of each lipid molecule studied and estimation of lipid diffusion area.

Lipid domains confine the membrane distribution of lipid molecules, thus increasing their local concentration. The encounter rate calculated in our method is the effective rate after taking diffusion confinement into consideration. In comparison, if each lipid molecule can freely diffuse along the whole cell membrane, the encounter rate will follow the two-dimensional Smoluchowski equation[11], where $F = 2\pi N_a C^2(D_1 + D_2)/\ln[(\pi N_a C)^{-1/2}/a]$. Here, "a" is the encounter radius two DNA probes must reach in order to react, and such radius is estimated to be around 5 nm for toehold-mediated strand displacement reactions[9,10]. "D_1" and "D_2" are the respective diffusion coefficients of each lipid molecule on the membrane. "C" is the concentration of lipids on the cell membrane, which was estimated to be about 0.19 pmol/cm^2. Based on this model, the encounter rate F can be calculated, as summarized in the following table.

	Free diffusion encounter rate (per μm^2 per sec)	Lipid diffusion area percentage of whole cell membrane
Diacyllipid / Diacyllipid	5.2 ± 0.7	(52 ± 7) %
Cholesterol / Cholesterol	7.3 ± 1.2	(39 ± 5) %
Tocopherol / Tocopherol	9.6 ± 1.6	(77 ± 8) %

Since the lateral distribution among different lipids demonstrates considerable variability, we only calculated the encounter rates between the same types of lipid. Since the existence of lipid domain confines the membrane distribution of lipid molecules, thus increasing their local effective concentration. Because of such increased effective concentration compared to that in the free diffusion mode, lipid membrane encounter rates (Table in Discussion 2) are all larger than free diffusion encounter rates (above Table).

© 2017 Macmillan Publishers Limited, part of Springer Nature. All rights reserved.

Based on the two-dimensional Smoluchowski equation[11], where $F = 2\pi N_a C^2(D_1+D_2)/\ln[(\pi N_a C)^{-1/2}/a]$, the square root of lipid membrane concentration, C, is proportional to membrane encounter rate, i.e., $F_{effective}/F_{free\ diffusion} \sim C^2_{effective}/C^2_{free\ diffusion}$ Here, $C_{free\ diffusion}$ represents lipid membrane concentration based on homogeneous lipid distribution over the whole area of cell membrane. When the total amount of lipids on each cell membrane is fixed, the membrane diffusion area is reciprocally proportional to the membrane concentration, i.e., $A_{effective}/A_{whole\ cell} = C_{free\ diffusion}/C_{effective} = \sqrt{F_{effective}}/\sqrt{F_{free\ diffusion}}$. Thus, we can estimate lipid diffusion area percentage over the whole cell membrane, $A_{effective}/A_{whole\ cell}$, based on the difference of effective encounter rate., $F_{effective}$ (Table in Discussion 2), with free diffusion encounter rate, $F_{free\ diffusion}$ (Table in Discussion 3).

© 2017 Macmillan Publishers Limited, part of Springer Nature. All rights reserved.

References

1. Liu, H. et al. DNA-based micelles: synthesis, micellar properties and size-dependent cell permeability. *Chemistry* **16**, 3791-3797 (2010).
2. Liu, H. & Johnston, A. P. A programmable sensor to probe the internalization of proteins and nanoparticles in live cells. *Angew. Chem. Int. Ed. Engl.* **52**, 5744-5748 (2013).
3. Engelman, D. M. Membranes are more mosaic than fluid. *Nature* **438**, 578-580 (2005).
4. Zidovetzki, R. & Levitan, I. Use of cyclodextrins to manipulate plasma membrane cholesterol content: evidence, misconceptions and control strategies. *Biochim. Biophys. Acta.* **1768**, 1311-1324 (2007).
5. Kang, M. et al. Simplified equation to extract diffusion coefficients from confocal FRAP data. *Traffic* **13**, 1589-1600 (2012).
6. Groves, J. T., Parthasarathy, R. & Forstner, M. B. Fluorescence imaging of membrane dynamics. *Annu. Rev. Biomed. Eng.* **10**, 311-338 (2008).
7. Yin, Y. & Zhao, X. Kinetics and dynamics of DNA hybridization. *Acc. Chem. Res.* **44**, 1172-1181 (2011).
8. Zhang, D. Y. & Winfree, E. Control of DNA strand displacement kinetics using toehold exchange. *J. Am. Chem. Soc.* **131**, 17303-17314 (2009).
9. Genot, A. J., Zhang, D. Y., Bath, J. & Turberfield, A. J. Remote toehold: a mechanism of flexible control of DNA hybridization kinetics. *J. Am. Chem. Soc.* **133**, 2177-2182 (2011).
10. Chandran, H., Gopalkrishnan, N., Phillips, A. & Reif, J. Localized hybridization circuits, *DNA17*, 64-83 Springer Verlag, (2011).
11. Hardt, S. L. Rates of diffusion controlled reactions in one, two and three dimensions. *Biophys. Chem.* **10**, 239-243 (1979).
12. Lukacs, G. L. et al. Size-dependent DNA mobility in cytoplasm and nucleus. *J. Biol. Chem.* **275**, 1625-1629 (2000).
13. Hannestad J. K. et al. Kinetics of diffusion-mediated DNA hybridization in lipid monolayer films determined by single-molecule fluorescence spectroscopy. *ACS Nano* **7**, 308-315 (2013).
14. Schade M. et al. Remote control of lipophilic nucleic acids domain partitioning by DNA hybridization and enzymatic cleavage. *J. Am. Chem. Soc.* **134**, 20490-20497 (2012).

© 2017 Macmillan Publishers Limited, part of Springer Nature. All rights reserved.